Influence of acoustic streaming on the stability of a laterally heated three-dimensional cavity

W. Dridi, D. Henry, and H. Ben Hadid
Laboratoire de Mécanique des Fluides et d'Acoustique, CNRS/Université de Lyon, École Centrale de Lyon/Université Lyon 1/INSA de Lyon, ECL, 36 avenue Guy de Collongue, 69134 Ecully Cedex, France

(Received 20 September 2007; revised manuscript received 18 January 2008; published 23 April 2008; publisher error corrected 29 April 2008)

The flows induced by acoustic streaming in a three-dimensional side-heated parallelepiped cavity of length A_x representative of crystal growth configurations are numerically studied. Both the structure of the flows and their stability properties are determined. The flows have different symmetries, belonging to the group D_4 for pure streaming, $Z_2 \times Z_2$ for pure buoyancy, and Z_2 for the mixed case, but these symmetries are generally broken at the first bifurcation points. Bifurcation diagrams are obtained which show that the flows become oscillatory periodic at a Hopf bifurcation, either directly on the primary steady solution branch, or on a secondary branch which bifurcates from the primary branch at a steady bifurcation point. The critical Grashof numbers for these bifurcation points are calculated as a function of the cavity length A_x, the Prandtl number Pr and the acoustic streaming parameter A. The thresholds are generally found to increase when the acoustic streaming contribution is enhanced, which indicates a stabilizing effect induced by acoustic streaming and may explain the observed improvement of the crystal quality when ultrasound waves are applied during the growth process. Destabilization effects are, however, found in some parameter range.

DOI: 10.1103/PhysRevE.77.046311 PACS number(s): 47.20.Bp, 47.20.Ky, 43.25.+y

I. INTRODUCTION

Acoustic streaming [1] describes a steady flow generated by a sound wave propagating in a fluid. It is a nonlinear effect which owes its origin to the action of Reynolds stresses and the dissipation of acoustic energy flux. There are two main types of acoustic streaming: Eckart streaming [2] (or quartz wind) in which the dissipation takes place in the main body of the fluid, and Rayleigh streaming [3] in which the dissipation is associated with boundary layers at solid surfaces. These streaming motions have been used to move fluids in microfluidic devices [4], enhance rate-limited processes such as diffusion [5] and heat transfer [6], induce chaotic mixing [7], and even improve solidification processes [8]. In this paper we consider Eckart streaming in which the flow, generated inside the ultrasound beam, moves away from the source within the body of fluid. As indicated by many authors [1,2,9,10], Eckart streaming can be modeled in the Navier-Stokes equations through a body force acting within the ultrasound beam. With this modeling, the acoustic streaming velocities have been determined analytically for a few simple systems [2,10,11]. In our case, we will consider a three-dimensional parallelepiped cavity and the problem will be solved by numerical simulation.

The present work is connected to the technologies of materials processing (semiconductors and metallic compounds such as InP, GaAs, In-Sb, Bi-Sb, In-Cd,…) by directional solidification from their melt. The motions inside the melt are generally complex and time dependent and they influence the quality of the obtained materials. The control of these motions has then become an important research objective for the last decade. In addition to microgravity and magnetic fields which are both costly and heavy technologies, the use of ultrasound waves seems to be promising. As already mentioned, such acoustic waves have been shown through experimental studies to be efficient in solidification situations [8], but the way they act through melt flow modifications is not yet clear. The objective of this work is then to determine the influence of acoustic streaming on these melt flows generated in differentially heated cavities, and more specifically on the instabilities which spontaneously appear in such flows [12]. The cavity considered in our numerical simulations is typical of horizontal crystal growth configurations.

II. MATHEMATICAL MODEL AND NUMERICAL TECHNIQUES

A. Mathematical model

The mathematical model consists of a rectangular parallelepiped cavity filled with a low-Prandtl number fluid $(0.001 \leq \mathrm{Pr} \leq 0.04)$ (Fig. 1). The cavity has aspect ratios $A_x = L/h$ $(2 \leq A_x \leq 5)$ and $A_y = l/h = 1$ (square cross section), where L is the length of the cavity (along x), h is its height (along z), and l is its width (along y). This cavity is heated from the side and submitted to an ultrasound beam.

The vertical end walls are isothermal and held at different temperatures, $\bar{T}_h$ at the right hot end wall and $\bar{T}_c$ at the left cold end wall, whereas the sidewalls are adiabatic. The fluid is assumed to be Newtonian with constant physical proper-

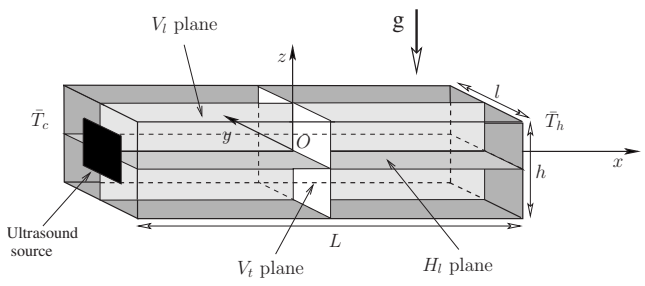

FIG. 1. Schematic diagram of the geometry.

ties (kinematic viscosity ν, thermal diffusivity κ, density ρ), except that, according to the Boussinesq approximation, the fluid density is considered as temperature dependent in the buoyancy term with a linear law $\rho=\rho_m[1-\beta(\bar{T}-\bar{T}_m)]$, where β is the thermal expansion coefficient, $\bar{T}_m$ is the mean temperature, $\bar{T}_m=(\bar{T}_h+\bar{T}_c)/2$, and ρ_m is the value of the density at $\bar{T}_m$.

The ultrasound beam is generated by an ultrasound source which is supposed to be square (of dimensionless size $H_b=h_b/h=0.62$) and located in the center of the left end wall. The divergence of the beam is assumed to be small, so that the beam can be considered to have a constant square cross section equal to that of the source. The ultrasound field is assumed to be a plane wave traveling in the positive x direction, with no reflection of the beam at the right end wall. This can be obtained by favoring a good transmission of the beam outside the cavity or by using an absorbing material. The attenuation of the acoustic wave in the viscous fluid, due to the dissipation of acoustic energy flux, generates a body force F acting within the ultrasound beam and equal to the spatial variation of the Reynolds stress [1,9]. The components of F are given by Lighthill [1] as $F_j=-\partial(\overline{\rho u_i' u_j'})/\partial x_i$, where i and j denote the three directions of space, x_i is the spatial coordinate in the i direction, the u_i' are the fluctuating velocities in the sound wave and the bar signifies a mean value in time. The equivalent vector expression of $\boldsymbol{F}$, which can be found, for example, in Nyborg [9] and Frampton *et al.* [4], is $\boldsymbol{F}=-\rho[\overline{(\boldsymbol{u}'\cdot\boldsymbol{\nabla})\boldsymbol{u}'+\boldsymbol{u}'(\boldsymbol{\nabla}\cdot\boldsymbol{u}')}]$. For a plane wave traveling in the positive x direction, the particle fluctuating velocity in the ultrasound beam can be written as $u_1'=V_a e^{-\alpha x}\sin(\omega t-kx)$, where ω, k, V_a, and α are the angular frequency, the wave number, the particle velocity amplitude, and the spatial attenuation factor of the sound wave, respectively. The force F is therefore oriented along the x axis and its intensity is given by $F=\rho\alpha V_a^2 e^{-2\alpha x}$ [9]. Now, provided the beam is only slightly divergent and the attenuation of the wave sufficiently weak, a body force which is constant ($F=\rho\alpha V_a^2$) inside the constant square cross-section beam and zero everywhere else in the cavity, can be defined [2,10,11]. Following Lighthill [1], this body force is introduced in the Navier-Stokes equations which, in our case, are coupled with an energy equation through the buoyancy term. Using h, h^2/ν, ν/h, $\rho\nu^2/h^2$, and $\gamma=(\bar{T}_h-\bar{T}_c)/A_x$ as scales for length, time, velocity, pressure, and temperature, respectively, these equations take the following form:

$$\boldsymbol{\nabla}\cdot\mathbf{u}=0, \tag{1}$$

$$\frac{\partial\mathbf{u}}{\partial t}+(\mathbf{u}\cdot\boldsymbol{\nabla})\mathbf{u}=-\boldsymbol{\nabla}p+\boldsymbol{\nabla}^2\mathbf{u}+\mathrm{Gr}T\mathbf{e}_z+A\delta_b\mathbf{e}_x, \tag{2}$$

$$\frac{\partial T}{\partial t}+(\mathbf{u}\cdot\boldsymbol{\nabla})T=\frac{1}{\mathrm{Pr}}\boldsymbol{\nabla}^2T, \tag{3}$$

with boundary conditions given by $\partial T/\partial z=0$ on $z=\pm 1/2$ and $\partial T/\partial y=0$ on $y=\pm A_y/2$, $T=-A_x/2$ on $x=-A_x/2$ and $T=A_x/2$ on $x=A_x/2$, and $\mathbf{u}=0$ on all boundaries. The dimensionless variables are the velocity vector $\mathbf{u}=(u,v,w)$, the pressure p and the temperature $T=(\bar{T}-\bar{T}_m)/\gamma$, and $\mathbf{e}_z$ and $\mathbf{e}_x$ are the unit vectors in the vertical and longitudinal directions, respectively. The nondimensional parameters are the Grashof number $\mathrm{Gr}=\beta g\gamma h^3/\nu^2$, the Prandtl number $\mathrm{Pr}=\nu/\kappa$ and the acoustic streaming parameter $A=\alpha V_a^2 h^3/\nu^2$ which is the dimensionless expression of the acoustic force F. δ_b is a function of the space coordinates and its value is 1 inside the ultrasound beam and 0 outside.

B. Numerical techniques

The governing equations of the model are solved in the three-dimensional domain using a spectral element method [13]. The time discretization is carried out using a semi-implicit splitting scheme where the nonlinear terms are first integrated explicitly, the pressure is then solved through a pressure equation enforcing the incompressibility constraint, and the linear terms are finally integrated implicitly. This time integration scheme is used for transient computations with a third-order accurate formulation. However, our main interest is in steady state solving and calculation of bifurcation points which are both done by Newton methods as described in Henry and Ben Hadid [14]. The main idea is to solve the linear systems appearing at each Newton step by an iterative solver, and to compute right-hand sides and matrix-vector products corresponding to these linear systems by performing adapted first order time steps of the basic or linearized problem. The Jacobian matrix is thus never constructed or stored. The generalized minimal residual (GMRES) algorithm is used as the iterative solver. Finally, in order to initiate the calculation of bifurcation points, we have to calculate leading eigenvalues—those with largest real part and thus responsible for initiating instability—and their corresponding eigenvectors. This is done through Arnoldi's method (ARPACK library) by time stepping the linearized equations, as described by Mamun and Tuckerman [15].

III. RESULTS

A. Symmetries of the flows

In the Boussinesq approximation, the steady convective flows obtained at moderate Gr (below the first transitions) and without acoustic field in such a parallelepiped cavity correspond to a simple unicellular circulation, where the flow is up the hot wall, across the top, down the cold wall and returning along the bottom [Fig. 2(a)]. These flows present different symmetries [12]: a reflection symmetry S_l with respect to the longitudinal vertical V_l plane (left-right symmetry) and a π-rotational symmetry S_r about the transverse y axis. The combination of these two symmetries gives a symmetry S_c with respect to the center point of the cavity ($S_c=S_l\cdot S_r$). The symmetry group generated by these symmetries is the group $Z_2\times Z_2\equiv D_2$.

When the ultrasound wave is applied, but without heating, the flow generated by acoustic streaming is in the positive x direction in the center of the cavity and returns along the lateral walls [Fig. 2(b)]. In this case, due to the square cross sections of the cavity and of the ultrasound beam, the symmetry group is the dihedral group D_4, which corresponds to

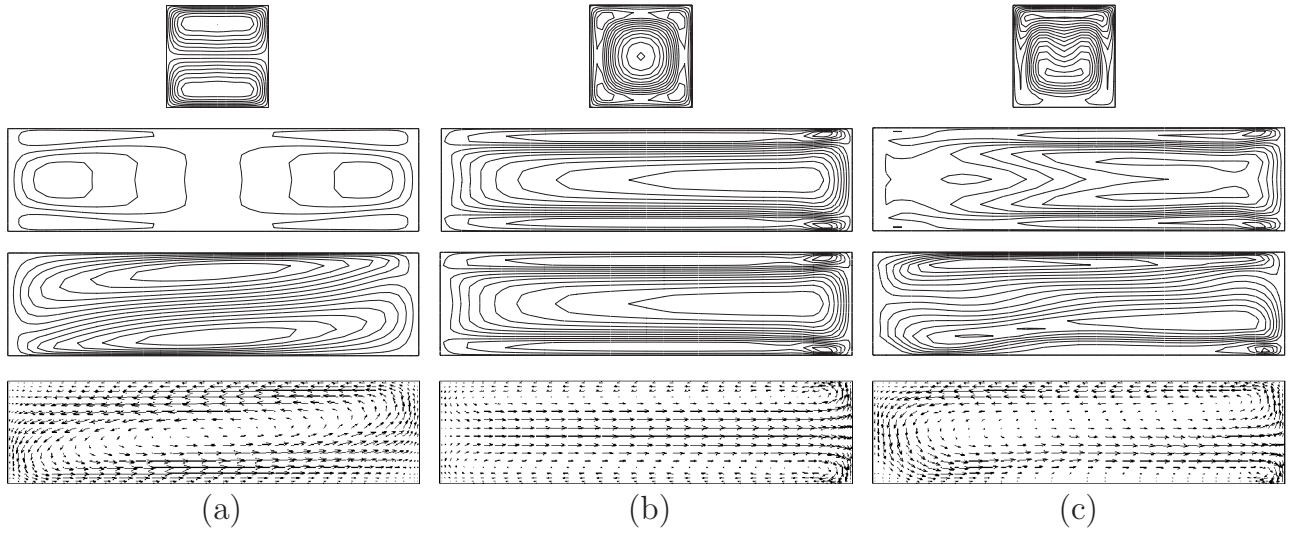

FIG. 2. Structure of the flows obtained with pure buoyancy [(a) Gr=40000, $A=0$], with pure acoustic streaming [(b) Gr=0, $A=40000$], then with combined buoyancy and acoustic streaming [(c) Gr=40000, $A=40000$] for $A_x=4$, $A_y=1$, $H_b=0.62$, and Pr=0.01. Contours of the longitudinal velocity field in the middle planes of the cavity (from top to bottom, V_t, H_l, and V_l planes), and then velocity vectors in the V_l plane.

reflection symmetries with respect to the V_l plane and to the longitudinal horizontal H_l plane, but also with respect to the longitudinal planes along the two diagonals of the square cross section. Finally, when the ultrasound wave is applied on the heated cavity, the flow is more complex, with only a reflection symmetry with respect to the V_l plane (symmetry group Z_2) [Fig. 2(c)], and its structure depends on the relative values of Gr (quantifying the buoyancy effect) and A (quantifying the acoustic streaming).

B. Bifurcation diagrams

We then study the first bifurcations which affect these flows. For that, we follow the primary flow solution branch by the continuation method and occasionally compute some of the leading eigenvalues by Arnoldi's method in order to locate changes of stability. If a steady bifurcation is located, the corresponding unstable eigenvector and the associated steady state solution are used to build a predictor for a solution along the emerging branch; the continuation method is then used to follow the new branch.

Figure 3 shows the bifurcation diagrams obtained for a cavity of aspect ratio $A_x=4$ for both $A=0$ and $A=40000$. (In this section, the Prandtl number is Pr=0.01.) The figure displays the evolution with Gr of the longitudinal velocity u at a given point in the cavity. For $A=0$ [pure buoyancy driven flow, Fig. 3(a)], the primary branch (with S_l and S_r symmetries) loses stability to steady perturbations breaking both S_l and S_r symmetries at $\mathrm{Gr}_c=61530$ (supercritical pitchfork bifurcation point S_1), producing a secondary branch of steady solutions with only the S_c symmetry. This secondary branch then becomes unstable at a Hopf bifurcation point O_2 at $\mathrm{Gr}_c=92696$. The Hopf bifurcation occurs without breaking of symmetry, so that beyond this point, a periodic oscillatory

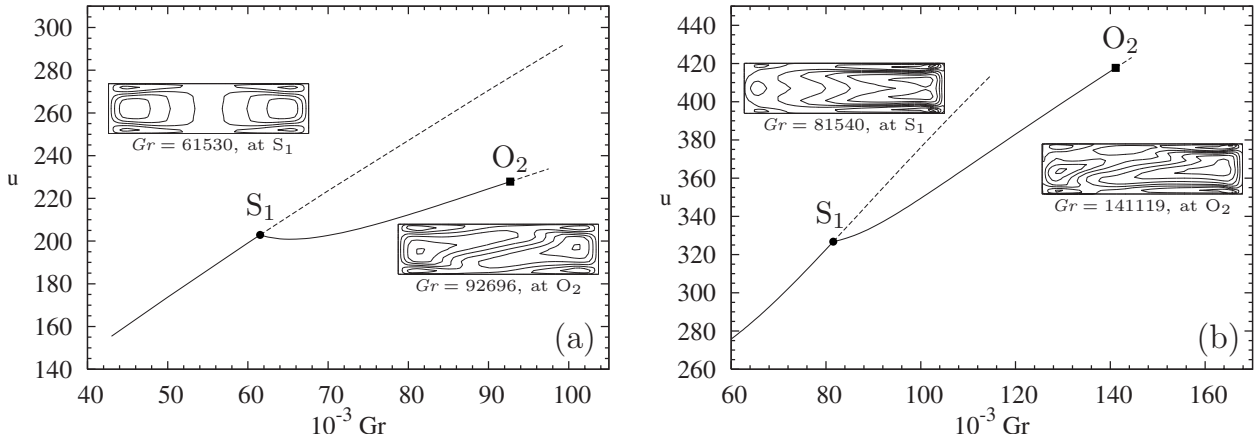

FIG. 3. Bifurcation diagrams for a laterally heated cavity ($A_x=4$, $A_y=1$, Pr=0.01): (a) without acoustic streaming, $A=0$; (b) with acoustic streaming, $A=40000$ ($H_b=0.62$). S_1 indicates a pitchfork bifurcation on the primary branch and O_2 a Hopf bifurcation on the bifurcated secondary branch. Insets are contours of the longitudinal velocity field in the H_l plane.

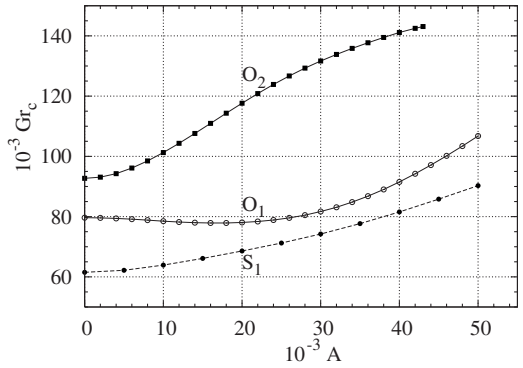

FIG. 4. Steady thresholds (S_1) on the primary branch of solutions and oscillatory thresholds (O_2) on the secondary branch for $A_x=4$ (see Fig. 3), and oscillatory thresholds (O_1) on the primary branch for $A_x=2.8$ as a function of the acoustic parameter A ($A_y=1$, $H_b=0.62$, Pr=0.01).

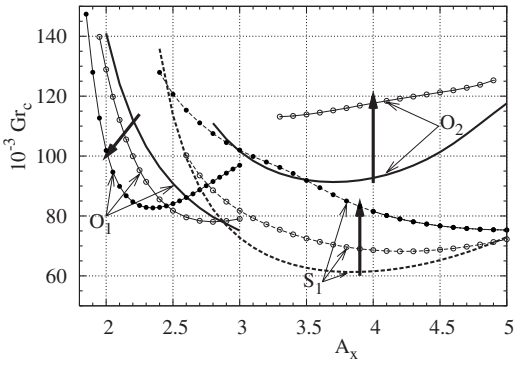

FIG. 5. Steady thresholds (S_1) on the primary branch of solutions, oscillatory thresholds (O_2) on the secondary branch, and oscillatory thresholds (O_1) on the primary branch as a function of the aspect ratio A_x for three values of the acoustic parameter, $A=0$ (thick lines), $A=20000$ (lines with circles), and $A=40000$ (lines with bullets) ($A_y=1$, $H_b=0.62$, Pr=0.01).

flow keeping the symmetry with respect to the center of the cavity can be observed. For $A=40000$ [combined buoyancy and acoustic streaming driven flow, Fig. 3(b)], the primary branch (with only the S_l symmetry) also loses stability with breaking of symmetry to a secondary branch of steady solutions. The corresponding supercritical pitchfork bifurcation occurs at $\mathrm{Gr}_c=81540$, a value larger than that obtained for $A=0$ indicating a stabilizing effect due to the acoustic streaming. This secondary branch of nonsymmetric states becomes then unstable at a Hopf bifurcation point at $\mathrm{Gr}_c=141119$ (still later than for $A=0$), beyond which a periodic oscillatory flow without symmetry can be observed.

Other calculations were done for a cavity of aspect ratio $A_x=2.8$. In this case, we find a direct transition from the primary branch to periodic oscillatory flows at a Hopf bifurcation point with breaking of the left-right S_l symmetry. For $A=0$, this transition occurs at $\mathrm{Gr}_c=79644$ and the oscillatory flow triggered keeps the S_r symmetry, whereas, for $A=40000$, the transition occurs at $\mathrm{Gr}_c=91509$ and beyond this point an oscillatory flow without symmetry can be observed. Note that, in this case too, the increase of A induces an increase of the threshold value.

C. Stability diagrams

We now describe more precisely and more widely the influence of acoustic streaming on the flow transitions. For that we continuously vary some of the important parameters of the problem (A, A_x, and Pr) and numerically compute the evolution of the different bifurcation points by continuation.

For the two previously considered aspect ratios ($A_x=4$ and $A_x=2.8$) and for Pr=0.01, we first vary the acoustic streaming parameter A. The results are displayed in Fig. 4 which shows the stability diagram giving the critical Grashof number Gr_c for the different transitions as a function of A. For $A_x=4$, in the studied domain of A, the critical values for both S_1 and O_2 transitions increase monotonously and quite strongly with A, the Hopf bifurcation evolving slightly more quickly. This indicates a clear stabilization of the buoyant flow by acoustic streaming in this case, which in particular allows to delay the onset of oscillatory flows responsible of damages in crystal growth. For $A_x=2.8$, however, the influence of acoustic streaming is more complex. The threshold for the Hopf bifurcation O_1 first slightly decreases with the increase of A until about $A=17000$, before a clear increase for larger values of A.

To have a better understanding on how the effect of acoustic streaming on the thresholds evolves with the aspect ratio A_x, we continuously vary the aspect ratio from about 2 to 5 and follow the important thresholds for three acoustic streaming intensities corresponding to $A=0$, $A=20000$, and $A=40000$. The results are shown in Fig. 5 through the plots of Gr_c for the different thresholds as a function of A_x. Without acoustic streaming ($A=0$, thick lines), the first bifurcation (smaller threshold on the primary branch) is steady (S_1 points) above $A_x=2.9$ ($2.9<A_x\leq 5$) and oscillatory (O_1 points) below this value ($2\leq A_x<2.9$). The influence of acoustic streaming on the S_1 bifurcation points is stabilizing, which confirms what was obtained for $A_x=4$ (Fig. 4). This influence is strong for $2.9<A_x<4$, but it strongly decreases when A_x is further increased. In the range of A_x where S_1 is the first bifurcation, the oscillatory transition (O_2 points) on the bifurcated secondary branch was also calculated. For this oscillatory transition too, the influence of acoustic streaming is stabilizing. It is the strongest for A_x around 4 and decreases when A_x goes to 5. Finally, in the range of A_x values where the first transition is oscillatory ($2\leq A_x<2.9$), the influence of acoustic streaming on the thresholds (O_1 points) is more complex. For A_x around 2, the influence is destabilizing in the whole range of A ($0\leq A\leq 40000$), whereas for A_x around 2.5, the initial destabilization is followed by a stabilizing effect. As A_x goes to 2.9, this stabilizing effect increases and the initial destabilization becomes weaker (see what is obtained for $A_x=2.8$ in Fig. 4).

We finally consider the influence of the Prandtl number, and thus vary Pr from 0.001 to 0.04 for a fixed aspect ratio $A_x=4$. The critical Grashof numbers for the different transitions are given as a function of Pr in Fig. 6. For the small values of Pr until about Pr=0.02, the first instability is steady (S_1 points) and the oscillatory transition (O_2 points) occurs on the bifurcated secondary branch. The influence of acous-

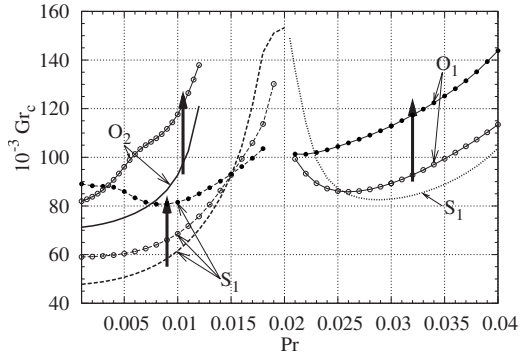

FIG. 6. Steady thresholds (S_1) on the primary branch of solutions, oscillatory thresholds (O_2) on the secondary branch, and oscillatory thresholds (O_1) on the primary branch as a function of the Prandtl number Pr for three values of the acoustic parameter, $A=0$ (thick lines), $A=20000$ (lines with circles), and $A=40000$ (lines with bullets) ($A_x=4$, $A_y=1$, $H_b=0.62$).

tic streaming on the S_1 transitions is stabilizing below Pr $=0.015$ but destabilizing for $0.015<\mathrm{Pr}<0.02$, whereas for the O_2 transitions, the influence, calculated only up to Pr $=0.012$, is found to be stabilizing. For the values of the Prandtl number above Pr$=0.02$, the dynamics of the flow without acoustic streaming ($A=0$) is very complex due to the presence of a saddle-node bifurcation point (denoted as S_1 and given as a thick short-dashed curve in Fig. 6) which appears before any other bifurcation when following the primary solution branch. A steady bifurcation with breaking of the S_r symmetry is detected farther on the primary branch (which progresses in the direction of decreasing Gr beyond the saddle-node point), indicating that the oscillatory transition might still be on a bifurcated secondary branch. The exact calculation of such bifurcation diagram which includes many subcritical branches is very difficult. It has been thought to be beyond the scope of this study which focuses on the acoustic streaming effect. Despite this lack of information for $A=0$, calculations have, however, been done for $A=20000$ and $A=40000$. We recall from Sec. III A that, when acoustic streaming is applied, the symmetry of the problem changes from $\mathbf{Z}_2\times\mathbf{Z}_2$ to $\mathbf{Z}_2$, with in particular the disappearance of the S_r symmetry. The steady bifurcation (originally with breaking of the S_r symmetry) then naturally disappears. Moreover, for the high values of A considered, we find that the saddle-node point too has disappeared. The bifurcation diagram for both $A=20000$ and $A=40000$ is then reduced to a simple direct transition from the primary branch to oscillatory flows at a Hopf bifurcation point. The variation with Pr of the critical Grashof number for this point O_1 is shown in Fig. 6 for both values of A. From the two curves, we see that, in this range of Pr ($0.02<\mathrm{Pr}<0.04$), there is still a stabilizing effect induced by acoustic streaming on the oscillatory transition, this effect decreasing when Pr goes to 0.02.

IV. RELEVANCE FOR REALISTIC EXPERIMENTAL SITUATIONS

In this section, we want to show the relevance of the acoustic model assumptions and of the nondimensional parameter values for realistic experimental situations. For the sake of simplicity, we choose a cavity with an aspect ratio $A_x=L/h=4$ and an ultrasound source of dimensionless size $H_b=h_b/h=2/3$. We will consider two situations: a first situation referred to as case (a) and corresponding to a cavity with $h=4.5$ cm (which implies $h_b=3$ cm and $L=18$ cm) and to an ultrasound wave of frequency $f=3$ MHz, and a second situation referred to as case (b) and corresponding to $h=1.5$ cm (which implies $h_b=1$ cm and $L=6$ cm) and to $f=10$ MHz.

A. Acoustic model assumptions

We first estimate the divergence of the acoustic beam. The half angle θ of a circular beam is defined by $\sin(\theta)=1.22c/(fh_b)$, where c is the sound velocity. To evaluate θ, we use the sound velocity of water $c\simeq 1500$ m/s, which is close to that in liquid metals. In both cases (a) and (b), we obtain small values of θ corresponding to slopes $\tan(\theta)$ equal to 2.05 and 2.31 %, respectively.

Concerning the spatial attenuation factor of the acoustic beam α, it depends on the dynamic viscosity μ which is also quite similar in water and in liquid metals. As we know that α is proportional to f^2 and that a characteristic value in water is $\alpha=0.01$ m^{-1} for $f=0.8$ MHz, we can write that $\alpha\sim 0.01(f/0.8)^2$, with f expressed in MHz. For the two cases previously considered, we get $\alpha=0.14$ and 1 m^{-1}, which gives rather weak 2.5 and 6 % attenuations on the corresponding lengths of the cavity.

B. Typical nondimensional parameter values

We want now to estimate the values of the nondimensional parameters which can be obtained in a realistic experiment and compare them with the characteristic values used in our numerical simulations. We still consider the two cases (a) and (b) and assume that the cavity is filled with gallium at a mean temperature of 346 K. The properties of gallium can be taken from the paper of Braunsfurth *et al.* [16]. At 346 K, we get $\rho=6089$ Kg/m^3, $\beta=1.3\ 10^{-4}$ K^{-1}, $\mu=1.75\ 10^{-3}$ Kg/m s, and $\nu=2.87\ 10^{-7}$ m^2/s, for the density, the thermal expansion coefficient, the dynamic viscosity, and the kinematic viscosity, respectively.

For an applied acoustic power P, we can define the acoustic intensity $I=P/h_b^2$, the particle velocity amplitude V_a such that $V_a^2=2\frac{P}{h_b^2}\frac{1}{\rho c}$, and finally the acoustic streaming parameter $A=\alpha V_a^2\frac{h^3}{\nu^2}$. For the case (a), for $P=0.5$ W, we get $A\simeq 18900$, and for the case (b), for $P=0.25$ W, we get $A\simeq 22400$. Concerning the Grashof number $\mathrm{Gr}=\beta g\frac{\Delta\bar{T}}{A_x}\frac{h^3}{\nu^2}$, where $\Delta\bar{T}$ is the applied temperature difference, $\Delta\bar{T}=0.2$ K leads to $\mathrm{Gr}\simeq 70300$ in case (a), whereas $\Delta\bar{T}=5$ K leads to $\mathrm{Gr}\simeq 65100$ in case (b).

From these examples, we see that the characteristic values used in the simulations for A (from 0 to 40000) and for Gr (from 60000 to 120000) can be reached in both situations for realistic experimental parameters. The experimental values of A and Gr can further be modulated by respectively adjusting the values of the applied acoustic power P and the ap-

plied temperature difference $\Delta\bar{T}$. We can, however, note that the case (a) would need a better control of the temperature in the cavity.

V. CONCLUSION

Our three-dimensional numerical simulations have shown that by applying an ultrasonic field to a laterally heated cavity, the flows generated by buoyancy are strongly changed through acoustic streaming effects and their stability properties are also deeply affected. The flows have different symmetry properties depending on whether buoyancy is considered alone or coupled to acoustic streaming. The bifurcation diagrams we have obtained by increasing the Grashof number both with or without acoustic streaming and for different cavity lengths and Prandtl numbers have shown that the transition to oscillatory flows is obtained either directly from the primary solution branch, or from a steady secondary branch which has previously bifurcated from the primary branch at a steady bifurcation point. A more complex behavior induced by a saddle-node bifurcation is also obtained in some parameter range for pure buoyancy, but acoustic streaming is found to simplify the dynamics in these cases and a direct transition to oscillations is finally obtained.

A main potentiality of our numerical tool is to allow the direct calculation of bifurcation points. We have then been able to follow the different bifurcation points by continuation over a large range of acoustic streaming parameters A, aspect ratios A_x, and Prandtl numbers Pr. The critical Grashof numbers for these bifurcation points are generally found to increase when the acoustic streaming contribution is enhanced. This effect is the strongest for aspect ratios ranging from $A_x=3$ to $A_x=4$ and for Prandtl numbers either small ($\mathrm{Pr} \leq 0.01$) or moderate ($0.025 \leq \mathrm{Pr} \leq 0.04$), and it decreases for larger aspect ratios. Such stabilizing effects induced by acoustic streaming may explain the observed improvement of the crystal quality when ultrasound waves are applied during the growth process. Destabilization effects are however found for small aspect ratios ($A_x \leq 2.5$) and for values of the Prandtl number around $\mathrm{Pr}=0.02$. This indicates that acoustic streaming has to be used with caution and with care.

ACKNOWLEDGMENTS

The calculations were carried out on NEC-SX5 and NEC-SX8 computers with the support of the CNRS through the "Institut du développement et des ressources en informatique scientifique."

[1] J. Lighthill, J. Sound Vibrat. **61**, 391 (1978).
[2] C. Eckart, Phys. Rev. **73**, 68 (1948).
[3] Lord Rayleigh, *The Theory of Sound* (MacMillan, London, 1929).
[4] K. D. Frampton, S. E. Martin, and K. Minor, Appl. Acoust. **64**, 681 (2003).
[5] J. D. Floros and H. Liang, Food Technol. **48**, 79 (1994).
[6] P. Vainshtein, M. Fichman, and C. Gutfinger, Int. J. Heat Mass Transfer **38**, 1893 (1995).
[7] C. Suri, K. Takenaka, H. Yanagida, Y. Kojima, and K. Koyama, Ultrasonics **40**, 393 (2002).
[8] G. N. Kozhemyakin, J. Cryst. Growth **149**, 266 (1995).
[9] W. L. Nyborg, in *Nonlinear Acoustics*, edited by M. F. Hamilton and D. T. Blackstock (Academic Press, San Diego, 1998), p. 207.
[10] O. V. Rudenko and A. A. Sukhorukov, Acoust. Phys. **44**, 653 (1998).
[11] W. Dridi, D. Henry, and H. Ben Hadid, C. R. Mec. **335**, 175 (2007).
[12] B. Hof, A. Juel, L. Zhao, D. Henry, H. Ben Hadid, and T. Mullin, J. Fluid Mech. **515**, 391 (2004).
[13] R. Touihri, H. Ben Hadid, and D. Henry, Phys. Fluids **11**, 2078 (1999).
[14] D. Henry and H. Ben Hadid, Phys. Rev. E **76**, 016314 (2007).
[15] C. K. Mamun and L. S. Tuckerman, Phys. Fluids **7**, 80 (1995).
[16] M. G. Braunsfurth, A. C. Skeldon, A. Juel, T. Mullin, and D. S. Riley, J. Fluid Mech. **342**, 295 (1997).